Available online at www.sciencedirect.com
ScienceDirect
Applied Surface Science 252 (2006) 8171–8177
applied surface science
www.elsevier.com/locate/apsusc

UV laser induced desorption of CsI and RbI ion clusters

F.A. Fernández-Lima [a,b], C.R. Ponciano [b], H.D. Fonseca Filho [b], E. Pedrero [c], M.A. Chaer Nascimento [d], E.F. da Silveira [b,*]

[a] *Instituto Superior de Tecnologias y Ciencias Aplicadas, Havana, Cuba*
[b] *Physics Department, Pontifícia Universidade Católica, Rua Marques de São Vicente 225, 22543-970 Rio de Janeiro, Brazil*
[c] *Facultad de Física-IMRE, Universidad de la Habana, Cuba*
[d] *Instituto de Química, Universidade Federal do Rio de Janeiro, Rio de Janeiro, Brazil*

Received 22 September 2005; received in revised form 23 October 2005; accepted 23 October 2005
Available online 22 November 2005

Abstract

Experimental results of laser sputtering of cesium and rubidium iodide secondary ions are presented. A TOF mass spectrometer, operating in linear mode, continuous extraction for positive or negative ions, was used for the analysis of $(CsI)_nCs^+$, $(CsI)_nI^-$, $(RbI)_nRb^+$ and $(RbI)_nI^-$ ion emission as a function of the laser irradiance. Experimental data show that the cluster ion emission yields decrease exponentially with n, for all the laser irradiances applied. Theoretical analysis of the clusters structure was performed using density functional theory at the B3LYP/LACV3P level, for the positive and negative cluster series. A quasi-equilibrium evolution of the clusters is proposed to extract a parameter characteristic of the cluster recombination process: the effective temperature. The hypothesis of the atomic species' recombination (during the expansion of a high density highly ionized cloud) leading to cluster formation is confirmed to some extent in a second set of experiments: the UV laser ablation of a mixed and non-mixed cesium iodide and potassium bromide targets. These experiments show that the emission yields contain contributions from both the recombination process and from the sample stoichiometry, even for high laser irradiances.

PACS: 79.20.Ds; 82.80.Ms; 52.50.Jm; 36.40.Wa; 36.40.Cg

Keywords: Laser ablation; CsI; RbI; Charged clusters; TOF

1. Introduction

Great instrumental developments have been accomplished with the introduction of the laser in the last three decades, but there is still a lacking of a satisfactory understanding of the chemical–physical phenomena involved in laser ablation. The most widely applications of pulsed laser ablation are pulsed laser deposition (PLD) [1,2] and laser desorption mass spectrometry (LD-MS) [3]. PLD is a common method to grow thin films of a wide range of materials, such as metals, superconductors, semiconductors and insulators. The chemical activity and stickiness of the deposited films are properties that depend on the energy distribution of the laser ablated species [4].

The LD-MS technique and its modifications, i.e. matrix assisted laser desorption ionization mass spectrometry MALDI-MS [5,6], have been widely applied in modern biological analysis as a powerful technique for routine mass identification. In the early 1990s, in order to provide a first order correction for the initial distributions of the emitted ions, the delayed extraction (DE) technique was introduced to improve mass resolution and sensitivity in time-of-flight (TOF) mass spectrometry coupled with LD or MALDI.

The most commonly used experimental methods for laser induced gas phase study are optical diagnostics, such as time-resolved emission spectroscopy [1,7], or laser-induced fluorescence [2]. However, these techniques are often limited to low mass species because of the lack of tabulated data. The initial ion velocity of the emitted species has been thoroughly investigated and it was concluded that the distribution of this

* Corresponding author. Tel.: +55 21 5299360; fax: +55 21 2599397/5123222.
E-mail address: enio@fis.puc-rio.br (E.F. da Silveira).

0169-4332/$ – see front matter © 2005 Elsevier B.V. All rights reserved.
doi:10.1016/j.apsusc.2005.10.034

quantity is one of the best tools to characterize the laser ablation in LD and MALDI processes [8–18]. The importance of the initial velocity analysis is two-fold: (i) the absolute value of the average initial velocity, in regard to a practical performance of MALDI or LD/DE–TOF systems, is needed for accurate calibration procedures, and (ii) the width of the initial velocity distribution is an important factor limiting the mass resolution of the technique. Several authors have made important contributions to the understanding of the fundamental aspects of laser ablation by probing different stages of the plasma with the DE technique [8–18]. Another technique that can be used to study cluster ion stability and internal energy of metastable secondary ions is the analysis by reflection (or filtering) of the daughter ions [19–21]. Though a great deal of data has been produced and discussed in the literature, there is still a lack of quantitative models that could be useful for achieving a better understanding of the particularities of the ion formation.

From the theoretical point of view, several approaches have been used to describe the laser ablation process: analytical models based on self-regulating absorption via inverse bremsstrahlung (IB) [22] are successful when the laser irradiance is high enough to fully ionize the plasma in the early stage of the pulse; models considering that the vapor absorption reduces the amount of material removed [23]; models assuming that photo-absorption (photo-ionization of the excited states) and collisional processes produce plasma [24]; models including the shielding of the target by IB [25]; and numerical models based on the solid heating and evaporation by laser, as well as vapor heating, ionization and expansion [26].

We have previously reported a thermal ablation model to describe the ion dynamics of the cesium ions created by UV laser in the first stages of their temporal evolution [27]. The model was used to describe the plume temperature evolution during its expansion using DE–TOF–MS spectra at different laser irradiances. Since a series of $(CsI)_nCs^+$ ($n = 0, 1, 2$) clusters is observed experimentally and since the cluster emission cannot be described by standard evaporation models, in a subsequent report [28], the secondary ion yields were described by the product of two terms: one representing the mechanism of energy absorption/deposition and the other being proportional to the probability of the atomic species' recombination during the expansion of the high density and highly ionized cloud.

In this paper, new experimental results of laser sputtering of cesium and rubidium iodide clusters are presented. A BRUKER/BIFLEX III TOF mass spectrometer was used in the linear mode to analyze sequentially positive and negative secondary ions. $(CsI)_nCs^+$, $(CsI)_nI^-$, $(RbI)_nRb^+$ and $(RbI)_nI^-$ ion emission was studied as a function of the laser irradiance. A theoretical search for the possible structures of these ion clusters using density functional theory at the B3LYP/LACV3P level was performed. The results are discussed on the basis of the concept of the effective temperature characteristic of the cluster recombination process. The hypothesis of the atomic species recombination during the expansion of a high density and highly ionized cloud leading to cluster formation is confirmed by comparing the analysis of UV laser induced sputtering of targets prepared with two alkaline halides (CsI and KBr), with different degrees of homogenization.

2. Experiment

2.1. Sample preparation

Cesium iodide (≥99.5% purity from Merck, Darmstadt) and Rubidium iodide (≥99.8% purity from Coinbrook Bucks, England) powders were evaporated on a stainless steel target plate of the BRUKER mass spectrometer. CsI and RbI polycrystalline films were grown by physical deposition in an evaporation chamber at a pressure of 10^{-5} mbar.

Two targets of cesium iodide and potassium bromide (≥99.5% purity from Isofar, Brazil) were prepared: (A) CsI and KBr (refereed hereafter as ''mixed''), using the standard dried droplet method of a 1:1 mixture of CsI and KBr in aqueous solution and (B) CsI + KBr (refereed hereafter as ''non-mixed''), prepared by evaporating CsI powder over a previously evaporated KBr powder on stainless steel target plate of the BRUKER mass spectrometer.

2.2. Target characterization

The optical characterization was performed using a home-made optical microscope (450×) coupled to a CCD camera. The AFM measurements were performed with a commercial microscope (Nanoscope III, Digital Instruments) operated in the tapping mode for the analysis of the topography. All the experiments were performed at room temperature and the relative air humidity was kept constant at 40%.

The UV absorption coefficient was measured in an HP8452A Hewlett-Packard Spectrophotometer. The optical density (A) can be expressed as $A = \varepsilon_{MA}Cd$, where ε_{MA} is the molar absorption coefficient, C the molar concentration and d is the optical path inside the quartz sample cell. The absorption coefficients at 337 nm of the pure samples are: $\varepsilon_{MA}(CsI) = 371\ mol^{-1}\ cm^{-1}$, $\varepsilon_{MA}(RbI) = 143\ mol^{-1}\ cm^{-1}$ and $\varepsilon_{MA}(KBr) = 1\ mol^{-1}\ cm^{-1}$. Since shift effects are expected in the absorption band of the hygroscopic materials CsI and RbI, we have preferred to measure the absorption coefficients of the salts directly in water solution. The best target thickness was decided empirically for our laser irradiance.

2.3. MS analysis

The experiments were performed in a BRUKER/BIFLEX III mass spectrometer (see Fig. 1). The continuous mode of ion extraction was used. The laser characteristics are: 337 nm (nitrogen laser), pulses of 3 ns FWHM, 200 μJ/pulse, spot diameter of 50 μm. Briefly, after the laser pulse, the start signal of the time of flight spectrum is generated by the photodiode. The ions are desorbed from the target surface and accelerated in the region delimitated by the grids d_1 and d_2, entering in the field free region L where they are separated as function of their mass to charge ratio. The ion time of flight is detected by a

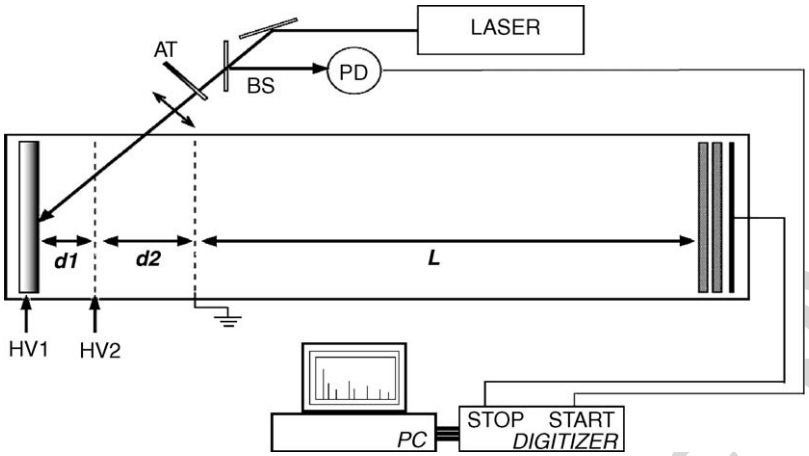

Fig. 1. Schematic diagram of the mass spectrometer. AT: gradient neutral density attenuator, BS: beam splitter, PD: photodiode, and HV1 and HV2: high voltage power supplies.

microchannel plate (MCP) located at the end of the field free region. The acceleration voltages are: HV1 = 19.0 kV and HV2 = 10.0 kV. The detection efficiency is corrected as function of the detector voltage.

3. Results and discussion

It is well known that the target preparation influences strongly the mass resolution of the observed species in LD-MS [8–18]. The amount of evaporated material is directly proportional to the laser irradiance and to the plume volume when using N_2 lasers (due to the 3 ns width of the laser pulse). Once the laser irradiance has been chosen as the reference parameter for the ionic species production and all the other parameters are kept constant (i.e. laser focus and MS acquisition set-up), the target thickness must be chosen according to two main conditions: (i) the target has to be thin enough to guarantee that the mass resolution will be kept constant and (ii) the target has to be thick enough to maintain desorption for multiple shots without reaching the stainless steel target plate. The second condition follows from the fact that the laser irradiance jitter (the laser energy dispersion) is minimized by averaging several shots. To fulfill these conditions, the CsI and RbI targets were grown to a thickness of about 400 and 830 nm, respectively, based on the values of their molar absorption coefficients. Despite the fact that the evaporated targets were kept in vacuum conditions, both been hygroscopic, water molecules are expected to be absorbed during the manipulation.

In laser ablation characterization studies, the homogeneity of the sample is a relevant parameter. Fig. 2 shows the optical (top) and AFM (bottom) images of the CsI (left) and RbI (right) evaporated targets. The crystallization of the samples strongly depends on the growth technique and it is known that the deposition by evaporation gives the best homogeneity, as can be observed. In the inset of Fig. 2 a fraction of the AFM image is amplified (10 μm × 10 μm). The evaporated targets of both CsI and RbI present polycrystalline structures. Note that the grain shapes are quite similar but are larger in the RbI target.

In Fig. 3, the positive and negative ion mass spectra, for CsI and RbI, are presented for $I_1 = 1.69$ GW/cm^2. The relative abundances of all the four different cluster series decreases exponentially. To study the cluster emission yield characteristics and get reasonable yields for large clusters, the laser irradiance was varied well above threshold for ion cluster production, i.e., with values which are typically one order of magnitude higher than MALDI experiments. As shown in Fig. 4, the relative abundances (normalized to $n = 1$) of the CsI and RbI ion clusters have a rough exponential decrease, independent of the applied laser irradiance. The laser irradiance was varied from $I_1 = 1.69$ to $I_5 = 0.39$ GW/cm^2. The cluster yield distributions can be fitted by exponential functions, $Y(I, m) = Y_0(I) \exp(-k_m m)$, where k_m is the slope parameter and m is the cluster mass. The values of the slope parameter k_m are: 0.009, for $(CsI)_nCs^+$, 0.012, for $(RbI)_nRb^+$, 0.007, for $(CsI)_nI^-$ and 0.008 for $(RbI)_nI^-$. It is worth to point out that, except for the first member ($n = 0$ is an atomic ion, not a cluster ion), both positive and negative ion series decrease exponentially with about the *same* slope. This is a clear evidence that the positive ion $(XY)_nX^+$ alkaline–halide series are formed by the same mechanism as the $(XY)_nY^-$ series: clusters are either residues of the fractured solid (coming from the cooler periphery of the laser spot) or produced by condensation in the plasma expansion. Of course, neutral clusters may also be emitted in the laser ablation but, pre-formed or condensed, they cannot be directly observed by the current set-up. The neutral species collide with ions in the plume producing recombination, which can be detected; collisions of ion–neutral and ion–ion are essentially the responsible for the recombination leading to the new species detected.

As we previously pointed out [28], a possible interpretation of such experimental exponential dependence of the species abundances on their masses could be as follows. Given the high temperature observed in the plasma produced by laser ablation [27,29,30], the primary stage of the plasma is mainly composed of atomic species. The gas temperature drops during its expansion, which leads to a recombination of the atomic species, i.e. the formation of the clusters.

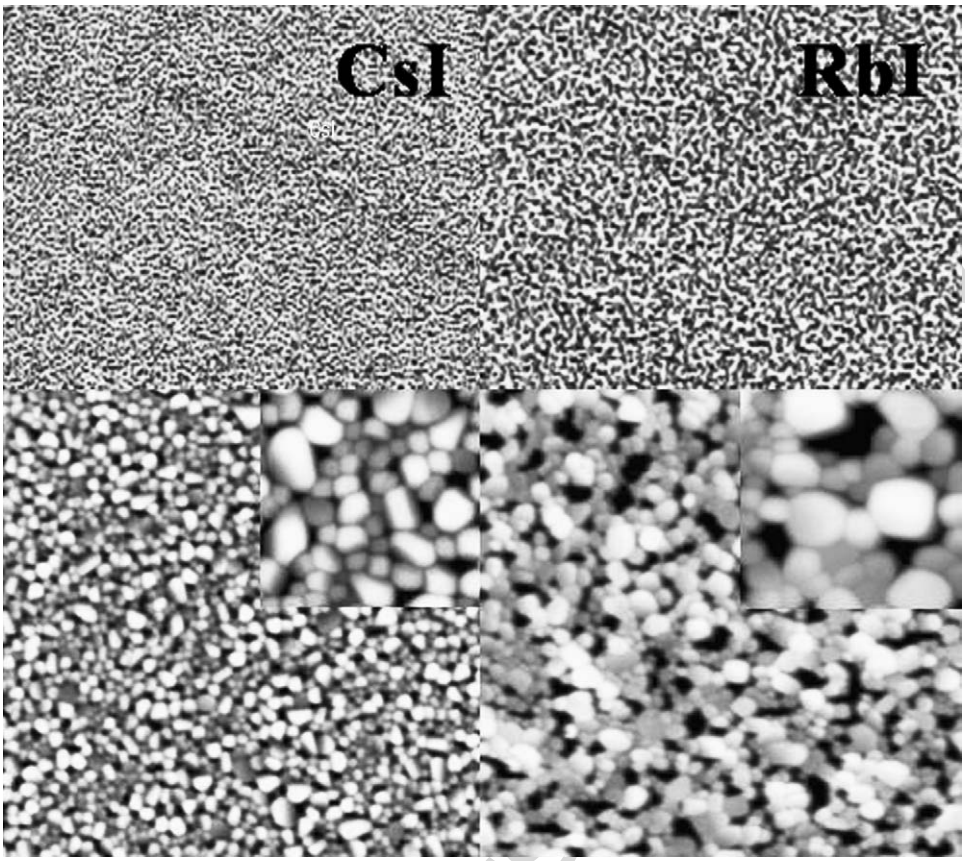

Fig. 2. Optical (top) and AFM (bottom) images of the CsI (left) and RbI (right) evaporated target. The optical and AFM images correspond to 450× and to 50 μm × 50 μm (inset of 10 μm × 10 μm), respectively.

The hypothesis of the atomic species' recombination during the expansion of a high density and highly ionized cloud, leading to cluster formation, is confirmed via two measurements: the UV laser induced sputtering of a ''mixed'' and a ''non-mixed'' targets of cesium iodide and potassium bromide (see inset of Fig. 5). If we assume that the laser ablation produces a high density ionized gas of atomic species, it is irrelevant whether the target is composed of two or four atomic species, both with the same stoichiometry and therefore produced in the same concentrations.

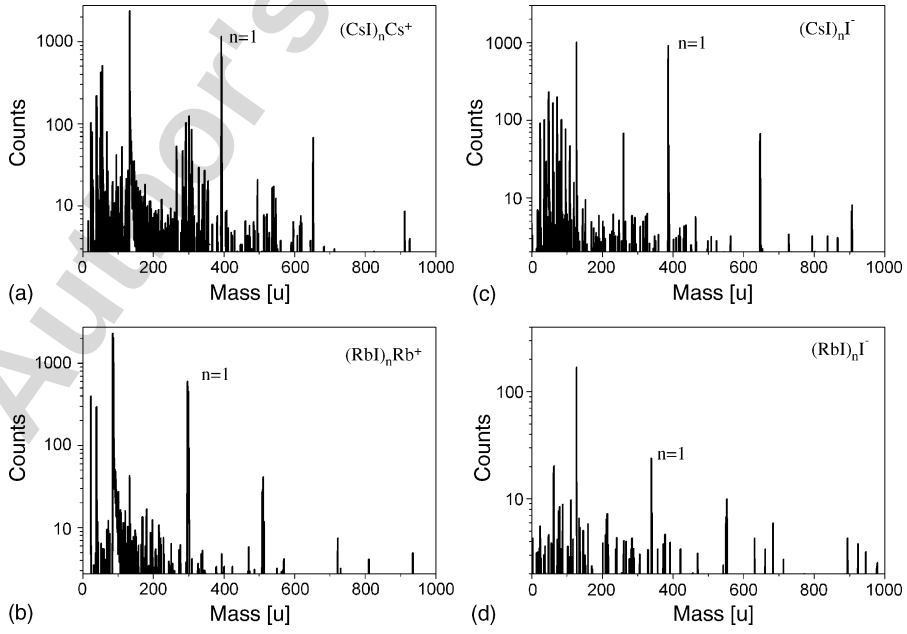

Fig. 3. Mass spectra showing the ion cluster series: (a) $(CsI)_nCs^+$, (b) $(RbI)_nRb^+$, (c) $(CsI)_nI^-$ and (d) $(RbI)_nI^-$.

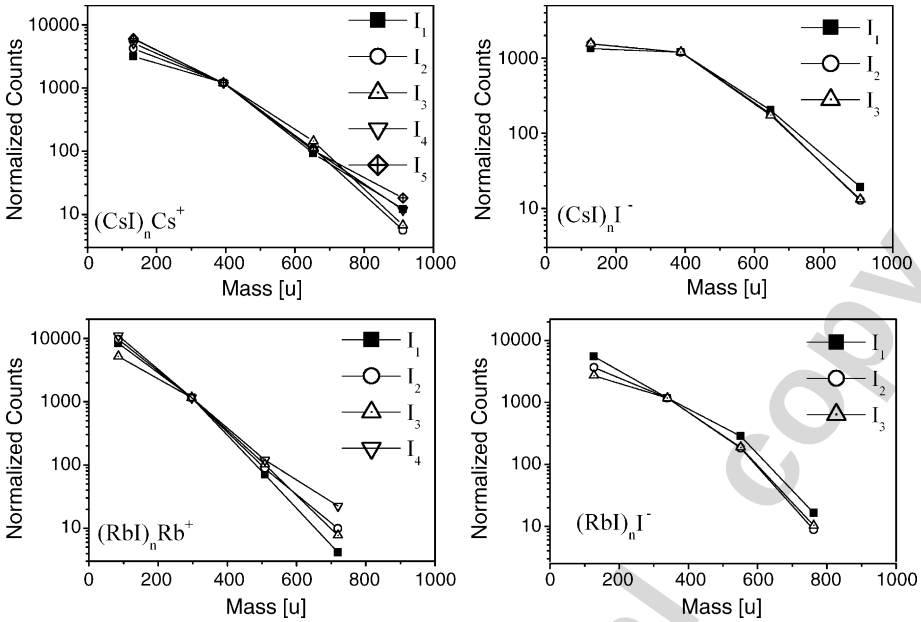

Fig. 4. Semi logarithmic plot of the relative abundances (normalized to $n = 1$) of the CsI and RbI positive and negative ion clusters. The intensity values are: $I_1 = 1.69$ GW/cm^2, $I_2 = 1.32$ GW/cm^2, $I_3 = 0.88$ GW/cm^2, $I_4 = 0.58$ GW/cm^2 and $I_5 = 0.39$ GW/cm^2.

In Fig. 5, the "mixed" A and "non-mixed" B samples mass spectra are presented. The "mixed" A mass spectrum represents an average of ten laser shots of $I = 0.3$ GW/cm^2. However, the "non-mixed" B mass spectrum was acquired with a single laser shot of $I = 4.5$ GW/cm^2. The higher laser intensity is to avoid residual laser modification of the target and also to guarantee the overall target evaporation, by producing a hole in a virgin spot of the target and completely removing all the material at once. Both experiments show that the same chemical combinations of tri-atomic ionic species are experimentally observed in both cases. Thus, the hypothesis of the atomic species' recombination leading to cluster formation proposed previously is confirmed.

Another information brought by Fig. 5 is that the experimental yields of each detected species of the A and B samples are of the same order of magnitude and that they can be fitted by the previously proposed exponential function $Y(I, m)$. In the case of the "mixed" sample A, the observed secondary ions $(CsI)K^+$, $(CsI)Cs^+$, $(KBr)K^+$ and $(KBr)Cs^+$, containing the original species CsI and KBr, are more abundant than those of the "non-mixed" B sample. This shows that, even when the sample was grown from an aqueous mixture of CsI and KBr powders, some history of the initial components (pre-formed) remains. Therefore, we cannot guarantee that the recombination process is complete and independent of the target characteristics, even for high laser irradiances. The cluster ion yield dependence on the laser intensity and on the target characteristics are being investigated [37].

Since the internal energy of the cluster varies almost linearly with its mass (see Fig. 6), the species' abundances can be written in terms of the clusters' energies [28]:

$$N_n(I) = C(I)\, \mathrm{e}^{-\beta^*(I)\varepsilon_n} \tag{1}$$

where N_n and ε_n represents the nth species abundance and energy, respectively, I the laser intensity, $C(I)$ a factor

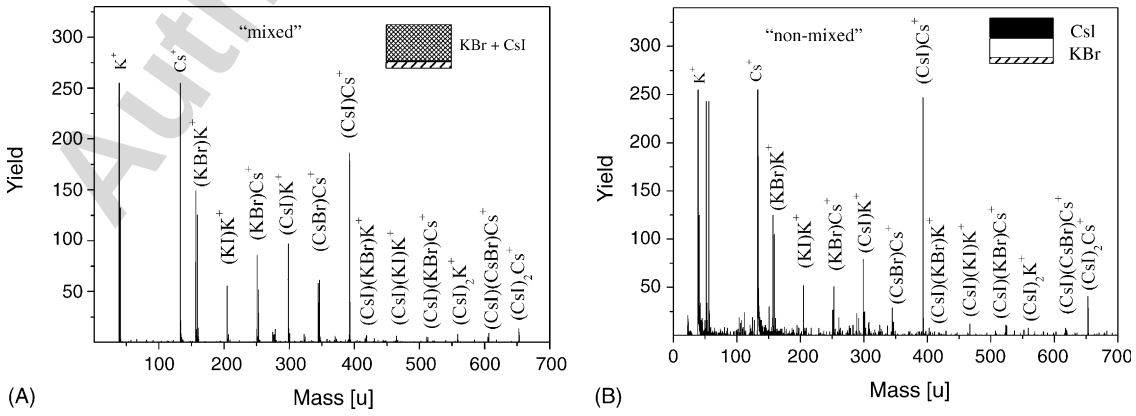

Fig. 5. Mass spectra of the "mixed" A and "non-mixed" B samples. In the inset a schematic view of the target composition is presented.

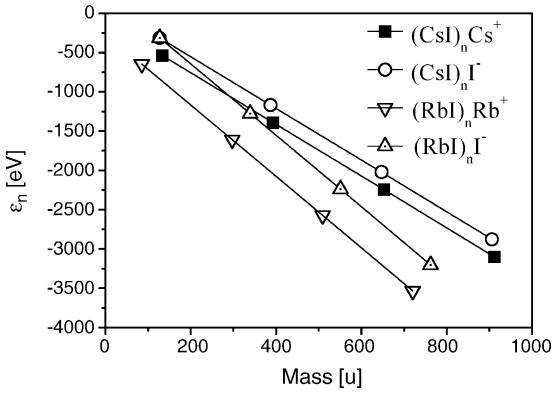

Fig. 6. Ion energy (ε_n) dependence on its mass. The energy values were calculated at the DFT/B3LYP/LACV3P level.

proportional to the laser irradiance, and $\beta^*(I) \propto 1/T^*(I)$ is a quantity that could be related to an effective temperature, T^*, characteristic of the recombination process in such conditions. This expression takes the form of a canonical distribution, which suggests the existence of a quasi-equilibrium evolution of the gas. The assumption of quasi-equilibrium evolution of the gas has been used by other authors [31–35].

Apparently, this quasi-equilibrium evolution arises due to a characteristic recombination rate larger than the gas expansion rate. Notice that the effective temperature is negative (different from the gas temperature), which is a characteristic of systems with an inverse state population. The species' abundance depends on the laser's intensity and varies during the gas expansion, up to the point where the free expansion is achieved (non-interacting system) and the recombination is not possible any longer. The effective temperature observed experimentally corresponds to the time when the free expansion regime is reached. From Fig. 3 it can be seen that the relative abundances do not depend on the laser intensity and consequently the effective temperature either. The N_n/N_{n+1} ratios depend on the experimental detection efficiency. For the analyzed systems, after correction of the detection efficiency, Eq. (1) could be re-written as:

$$N_n(I) = C(I)\,\mathrm{e}^{-\beta^*\varepsilon_n} \tag{2}$$

In order to determine the β^* value, characteristic of the recombination process, the energy of the clusters were calculated at the DFT B3LYP/LACV3P level, using the Jaguar 5.5 software [36]. A vibrational analysis on the optimized structures revealed that all the frequencies are real, indicating that these structures correspond to true minima on the potential hypersurfaces.

Table 1
Ion–ion distances and angles of the optimized structures as label in Fig. 7

XY	$(XY)_1X$ or $(XY)_1Y$	$(XY)_2X$ or $(XY)_2Y$	$(XY)_3X$ or $(XY)_3Y$
	$A_{123} = 180^\circ$	$A_{123} = 83^\circ$ $A_{143} = 94^\circ$ $A_{125} = 137^\circ$	$A_{214} = A_{413} = A_{312} = 86^\circ$ $A_{517} = A_{716} = A_{615} = 80^\circ$ $A_{215} = 45^\circ$ $DA_{1243} = -57^\circ$ $DA_{1567} = -61^\circ$
CsI	$d_{12} = d_{23} = 3.7$	$d_{12} = d_{23} = 4.0$ $d_{34} = d_{14} = 3.7$ $d_{25} = 3.8$	$d_{12} = d_{13} = d_{14} = 3.9$ $d_{15} = d_{16} = d_{17} = 5.4$
RbI	$d_{12} = d_{23} = 3.5$	$d_{12} = d_{23} = 3.8$ $d_{34} = d_{14} = 3.5$ $d_{25} = 3.6$	$d_{12} = d_{13} = d_{14} = 3.7$ $d_{15} = d_{16} = d_{17} = 5.1$

Table 2
The characteristic parameter $1/\beta^*$ of the recombination process

Cluster series	$1/\beta^*$ value (eV^{-1})		
	Cs^+	Rb^+	I^-
$(CsI)_n$	358 ± 39		457 ± 20
$(RbI)_n$		382 ± 43	569 ± 97

The optimized geometries for the positive and negative ion cluster series are presented in Fig. 7. The positive and negative clusters show exactly the same type of structure for $n = 1, 2$ and 3. The calculated bond angles are the same for both the Cs and Rb clusters but the inter-atomic distances (RbI and CsI) are slightly different. These geometrical parameters are presented in Table 1.

In Fig. 6, the ion energy (ε_n) includes the zero point energy correction. As can be observed, the mass of the cluster is proportional to its DFT energy. Once the clusters' energies are known, the value of β^* can be determined from the ratio of the species abundance, for any two members of the clusters series. The $1/\beta^*$ values are presented in Table 2. The parameter $1/\beta^*$ for the positive ions is smaller than for the negative ions, for both species. This fact could be related to the secondary electrons motion during the ion recombination because when the positive ions are analyzed, the applied electric field pushes the emitted electrons back to the target, provoking more collisions and certainly more ionization. When the negative ions are analyzed, the secondary electrons are quickly removed from the plume, thus reducing the number of electron–ion collisions and making the recombination process rarer than in the case of positive ions. However, this effect occurs mainly at the plume periphery and

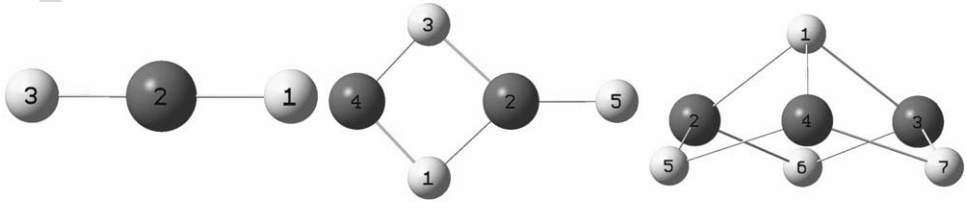

Fig. 7. Some optimized geometries for the positive and negative $(XY)_nX$ cluster series (where X = Cs or Rb and Y = I and vice versa).

only predominates during the high density and highly charged gas expansion because of the plume shielding against the external electric field.

4. Conclusions

$(CsI)_nCs^+$, $(CsI)_nI^-$, $(RbI)_nRb^+$ and $(RbI)_nI^-$ ion emission as a function of the laser irradiance is analyzed. Experimental data show that the positive and negative cluster ion emission yields decrease exponentially with n, for all applied laser irradiances. Theoretical analysis of the clusters structure was performed using the density functional theory at the B3LYP/LACV3P level, for the positive and negative cluster series. A quasi-equilibrium evolution of the clusters is proposed to extract a parameter characteristic of the cluster recombination process: the effective temperature. The hypothesis of the atomic species' recombination, during the expansion of a high density and highly ionized cloud, leading to cluster formation is confirmed, to some extent, by the UV laser ablation of a mixed and non-mixed cesium iodide and potassium bromide targets. The emission yields contains contributions from both the recombination process (characteristic of the cluster series) and from the sample characteristics (pre-formed species), even for high laser irradiances.

Acknowledgments

The authors would like to acknowledge the Brazilian Agencies CNPq, Faperj and CLAF for their support.

References

[1] N.R. Barnes, R. Dat, D.J. Lichtenwalner, A.F. Schreiner, O. Auciello, O.E. Hankins, Chem. Mater. 7 (1995) 477.
[2] C.E. Otis, R.W. Dreyfus, Phys. Rev. Lett. 67 (1991) 2102.
[3] A. Mele, D. Consalvo, D. Stranges, A. Giardini-Guidoni, R. Teghil, Int. J. Mass Spectrom. Ion Process 95 (1990) 359.
[4] D.B. Chrisey, G.K. Hubler (Eds.), Pulsed Laser Deposition of Thin Films, Wiley, New York, 1994.
[5] R.C. Beavis, B.T. Chait, Chem. Phys. Lett. 181 (1991) 479.
[6] T. Huth-Fehre, C.H. Becker, Rapid Commun. Mass Spectrom. 5 (1991) 378.
[7] T. García, E. de Posada, L. Ponce, J.L. Sánchez, S. Díaz, E. Pedrero, F. Fernández, P. Bartolo-Pérez, J.L. Peña, R. Diamant, J.A.M. Pereira, Mater. Lett. 49 (2001) 294–298.
[8] Y. Choi, H. Im, K. Jung, Int. J. Mass Spectrom. 189 (1999) 115.
[9] Y. Choi, H. Im, K. Jung, Appl. Surf. Sci. 150 (1999) 152.
[10] D.C. Barbacci, R.D. Edmondson, D.H. Russell, Int. J. Mass Spectrom. Ion Process 165 (1997) 221.
[11] M.L. Vestal, P. Juhasz, J. Am. Soc. Mass Spectrom. 9 (1998) 892.
[12] P. Juhasz, M.L. Vestal, S.A. Martin, J. Am. Soc. Mass Spectrom. 8 (1997) 209.
[13] M. Glückmann, M. Karas, J. Mass Spectrom. 34 (1999) 467.
[14] Y.-K. Choi, H.-S. Im, K.-W. Jung, Int. J. Mass Spectrom. 189 (1999) 115.
[15] Y.-K. Choi, H.-S. Im, K.-W. Jung, Appl. Surf. Sci. 150 (1999) 152.
[16] S. Berkenkamp, C. Menzel, F. Hillenkamp, K. Dreisewerd, J. Am. Soc. Mass Spectrom. 13 (2002) 209.
[17] I. Fournier, A. Brunot, J.C. Tabet, G. Bolbach, Int. J. Mass Spectrom. 213 (2002) 203.
[18] F. Fernández-Lima, V.M. Collado, C.R. Ponciano, L.S. Farenzena, E. Pedrero, E.F. da Silveira, Braz. J. Phys. 35 (2005) 170–174.
[19] C.R. Ponciano, F.E. Ávalos, A. Renteria, E.F. da Silveira, Int. J. Mass Spectrom. 209 (2001) 197–208.
[20] C.R. Ponciano, E.F. da Silveira, J. Phys. Chem. A 106 (2002) 10139–10143.
[21] C.R. Ponciano, R.C.C. Ladeia, V.M. Collado, E.F. da Silveira, Braz. J. Phys. 31 (2001) 314.
[22] F. Piuz, Nucl. Instrum. Meth. Phys. Res., Sect. A 371 (1996) 96–115.
[23] S. Fähler, H.U. Krebs, Appl. Surf. Sci. 96–98 (1996) 61.
[24] D.I. Rosen, J. Mitteldorf, G. Pugh, J. Appl. Phys. 53 (1982) 3190.
[25] J. Almeida, A. Amadon, P. Besson, P. Bourgeois, A. Braem, A. Breskin, A. Buzulutskov, R. Chechik, C. Coluzza, A. Di Mauro, J. Friese, J. Homolka, F. Iacovella, A. Ljubici Jr., G. Margaritondo, Ph. Miné, E. Nappi, T. dell'Orto, G. Paic, F. Piuz, F. Posa, J.C. Santiard, P. Sartori, S. Sgobba, G. Vasileiadis, T.D. Williams, Nucl. Instrum. Meth. Phys. Res., Sect. A 367 (1995) 332–336.
[26] A. Breskin, Nucl. Instrum. Meth. Phys. Res., Sect. A 371 (1996) 116–136.
[27] F. Fernández-Lima, V.M. Collado, C.R. Ponciano, L.S. Farenzena, E. Pedrero, E.F. da Silveira, Appl. Surf. Sci. 217 (2003) 202–209.
[28] V.M. Collado, F.A. Fernández-Lima, C.R. Ponciano, M.A. Chaer Nascimento, L. Velazquez, E.F. da Silveira, Phys. Chem. Chem. Phys. 7 (2005) 1971–1976.
[29] J.G. Lunney, R. Jordan, Appl. Surf. Sci. 127–129 (1998) 941–946.
[30] J.G. Lunney, R. Jordan, Appl. Surf. Sci. 127–129 (1998) 968–972.
[31] R. Kelly, R.W. Dreyfus, NIM B 32 (1988) 341.
[32] R. Kelly, R.W. Dreyfus, Surf. Sci. 198 (1988) 263.
[33] L.V. Zhigelei, B.J. Garrison, Appl. Phys. Lett. 71 (1997) 551.
[34] W. Zhang, B.T. Chait, Int. J. Mass Spectrom. Ion Process 160 (1997) 259–267.
[35] A.A. Puretzky, D.B. Geogehan, G.B. Hurst, M.V. Buchanan, Phys. Rev. Lett. 83 (N2) (1999) 444–447.
[36] Jaguar 5.5, Schroedinger Inc., Portland, OR, 2004.
[37] F.A. Fernandez-Lima, C.R. Ponciano, E.F. da Silveira, in press.